Atomic scale Monte-Carlo simulations of neutron diffraction experiments on UO_2 up to 1664 K

WPEC Subgroup 48 meeting via Zoom, May 12, 2021

S. XU[1] G. NOGUERE[1] L. DESGRANGES[1] J.-I. M. DAMIAN[2]

[1]CEA DES IRESNE Cadarache, Saint-Paul-lez-Durance, France; [2]Centro Atómico Bariloche, CNEA, Argentina

Table of Contents

Table of Contents

Neutron scattering cross section of $^{238}U^{16}O_2$

$$\sigma_{t_U}(E) = \sigma_{\gamma_U}(E) + \sigma_{n_U}(E) + \sigma_{f_U}(E) \qquad \sigma_{t_O}(E) = \sigma_{\gamma_O}(E) + \sigma_{n_O}(E) \quad (1)$$

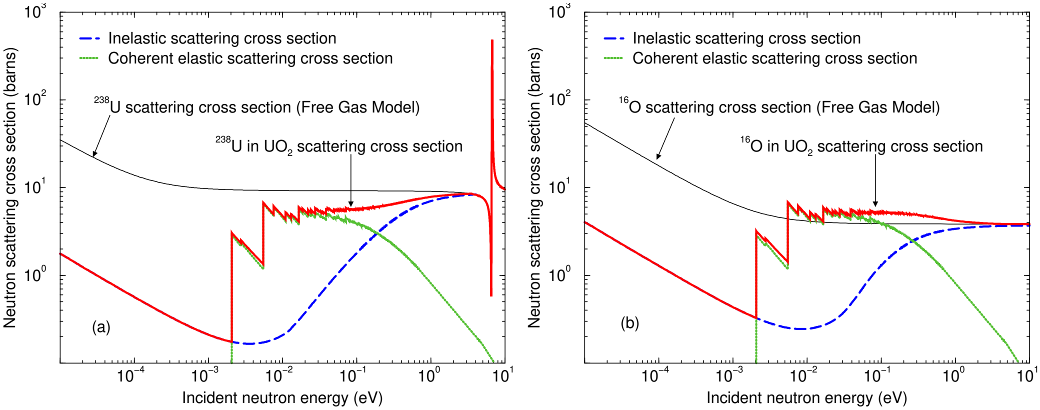

Double differential cross section & scattering function

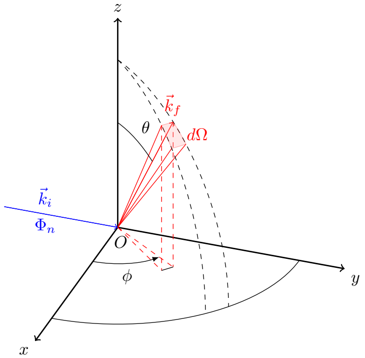

Figure: Schematic representation of low energy neutron scattering process.

At low neutron energy range (usually less than a few eV), the scattering of neutron in materials can be described via the double differential cross section (DDXS)

Cai and Kittelmann (2020); Schober (2014); Squires (2012)

$$\frac{d^2\sigma_{\vec{k}_i \Rightarrow \vec{k}_f}}{d\Omega \, dE_f} \equiv \frac{n(d\Omega,\, dE_f)}{\Phi_n \, d\Omega \, dE_f} = \frac{k_f}{k_i} S(\vec{Q},\, \omega) \tag{2}$$

$S(\vec{Q},\, \omega)$ is the scattering function defined by

$$S(\vec{Q},\, \omega) \equiv \frac{1}{2\pi\hbar} \sum_{j,j'=1}^{N} \overline{b_{j'} b_j} \int_{-\infty}^{\infty} \langle j',\, j \rangle \exp(-i\omega t)\, dt. \tag{3}$$

Harmonic approximation:

$$\langle j', j\rangle = \exp(-i\vec{Q}\cdot(\vec{d}_{j'} - \vec{d}_j))\exp(-W_{j'}(\vec{Q}))\exp(-W_j(\vec{Q}))\exp(\langle(\vec{Q}\cdot\vec{\boldsymbol{u}}_{j'}(0))(\vec{Q}\cdot\vec{\boldsymbol{u}}_j(t))\rangle). \quad (4)$$

Incoherent approximation:

$$\langle(\vec{Q}\cdot\vec{\boldsymbol{u}}_{j'}(0))(\vec{Q}\cdot\vec{\boldsymbol{u}}_j(t))\rangle = 0 \quad \text{if } j \neq j'. \quad (5)$$

Taylor expansion (phonon expansion Sjolander (1958)):

$$\exp(\langle(\vec{Q}\cdot\vec{\boldsymbol{u}}_j(0))(\vec{Q}\cdot\vec{\boldsymbol{u}}_j(t))\rangle) = \sum_{n=0}^{\infty}\frac{1}{n!}\left(\langle(\vec{Q}\cdot\vec{\boldsymbol{u}}_j(0))(\vec{Q}\cdot\vec{\boldsymbol{u}}_j(t))\rangle\right)^n. \quad (6)$$

Cubic approximation:

Phonon density of states (PDOS)

$$\langle(\vec{Q}\cdot\vec{\boldsymbol{u}}_j(0))(\vec{Q}\cdot\vec{\boldsymbol{u}}_j(t))\rangle = \frac{\hbar Q^2}{2M_j}\int_0^{\infty}\frac{\rho_j(\omega)}{\omega}\left(\coth(\frac{\hbar\omega}{2k_BT})\cos(\omega t) + i\sin(\omega t)\right)d\omega. \quad (7)$$

$$\text{For uranium dioxide: } \sigma_{n_j}(E) = \sigma^{\text{el}}_{\text{coh}}(E) + \sigma^{\text{inel}}_{j}(E) \tag{8}$$

where $\sigma^{\text{el}}_{\text{coh}}(E)$ represents the coherent elastic cross section (MF=7, MT=2 in ENDF-6 format Trkov and Brown (2018))

$$\sigma^{\text{el}}_{\text{coh}}(E) = \frac{\pi^2\hbar^2}{mNV_{\text{unit cell}}E} \sum_{hkl}^{E \geq E_{hkl}} d_{hkl} \left|F(\vec{\tau}_{hkl})\right|^2 \mathcal{P}_{hkl}(\vec{\text{PO}}, \vec{\tau}_{hkl}) \tag{9}$$

where

$$F(\vec{\tau}_{hkl}) = \sum_{j=1}^{N_{\text{unit cell}}} \overline{b_j} \exp\left(-\frac{\hbar^2\tau^2_{hkl}}{4M_j k_B T}\Lambda_j(T)\right) \exp\left(i\vec{\tau}_{hkl}\cdot\vec{p}_j - i\delta_{j\text{O}}\, c^{\text{O}}_{123}\,\tau^3_{hkl}\right) \tag{10}$$

and the inelastic cross section $\sigma^{\text{inel}}_{j}(E)$ can be obtained by integrating its double differential form

$$\frac{\mathrm{d}^2\sigma^{\text{inel}}_{j}}{\mathrm{d}\Omega\,\mathrm{d}E_f} = \frac{\sigma_{b,j}}{4\pi k_B T}\sqrt{\frac{E_f}{E_i}}\, S^{\text{inel}}_{j}(\alpha_j, \beta) \tag{11}$$

where $S^{\text{inel}}_{j}(\alpha_j, \beta)$ is dimensionless thermal scattering laws (TSLs) (MF=7, MT=4).

Table of Contents

Overview of TSL processing codes/platforms

Codes or platforms capable of calculating the thermal scattering laws (TSLs) of crystalline materials

- LEAPR MacFarlane (1994) module of NJOY code Macfarlane, Muir, Boicourt, Kahler III, and Conlin (2017)
- Monte-Carlo based library NCrystal Cai and Kittelmann (2020); Cai, Kittelmann, Klinkby, and Márquez Damián (2019)
- OCLIMAX platform Cheng, Daemen, Kolesnikov, and Ramirez-Cuesta (2019); Cheng and Ramirez-Cuesta (2020)
- Full law analysis scattering system hub (FLASSH) Zhu and Hawari (2018)

Table: Comparison of codes or platforms which enable to calculate the TSLs of crystalline materials

Codes/Platforms	LEAPR+NCrystal	OCLIMACX	FLASSH	CINEL (this work)
Harmonic approximation	Yes	Yes	Yes	Yes
Incoherent approximation	Yes	1-p correct	1-p correct	Yes
Cubic approximation	Yes	No	No	Yes
Support any material	Yes	Yes	Yes	Yes
SCT approximation	Yes	No	No	No
GPU speedup	No	not reported	not reported	Yes

Implementation & Python speedup of CINEL

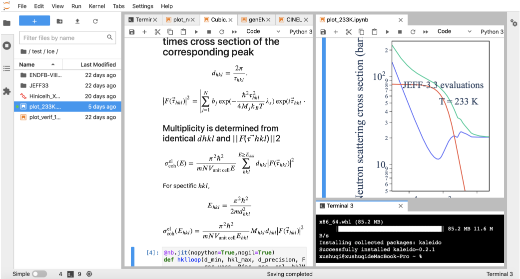

Figure: JupyterLab interface. Live code, texts, formatted mathematical equations and interactive graphics are mixed in Jupyter Notebooks which are integrated in JupyterLab together with blocks like terminal and text editor.

Table: Comparison of the computational time of the calculations of the TSL of H in H_2O at room temperature with phonon expansion order $N_{phonon} = 2000$. (Special thanks to our colleague P. TAMAGNO for providing his GPUs for test.)

	CPU	GPU K20	GPU K6000
GPU memory (gigabyte)	N/A	2	12
CUDA cores	N/A	384	2280
Computational time	$\sim$ 3 h	$\sim$ 15 min	$<$ 2 min

Ideal fluorite structure, $Fm\overline{3}m$ symmetry

Ong et al. (2013)

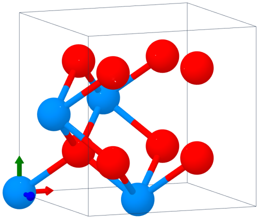

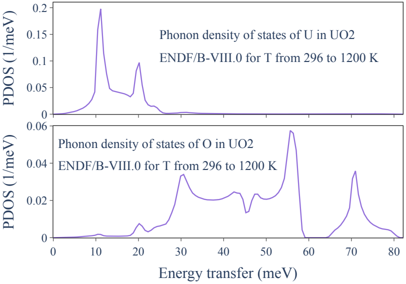

$\sigma_{coh}^{el}(E)$ decrease with T

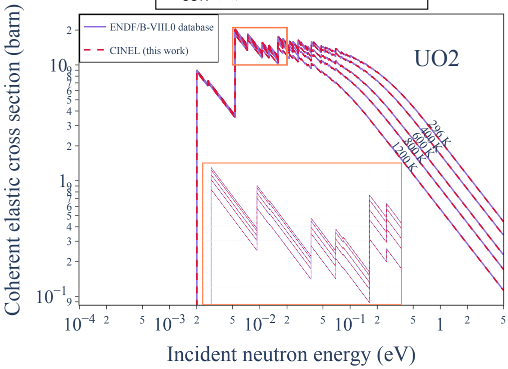

Wormald, Fleming, Hawari, and Zerkle (2021)

Numerical validations of CINEL: ^{238}U in UO_2

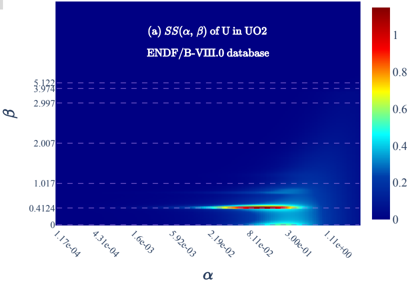

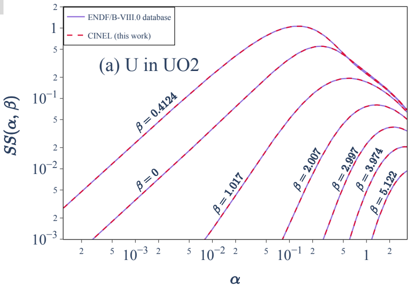

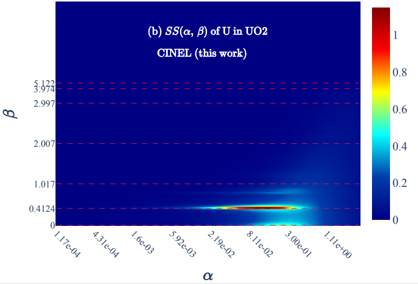

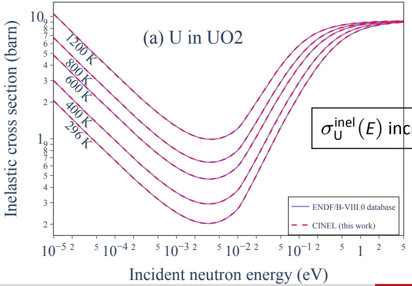

$\sigma_{U}^{inel}(E)$ increase with T

Numerical validations of CINEL: ^{16}O in UO_2

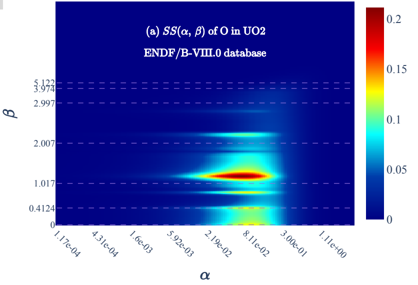

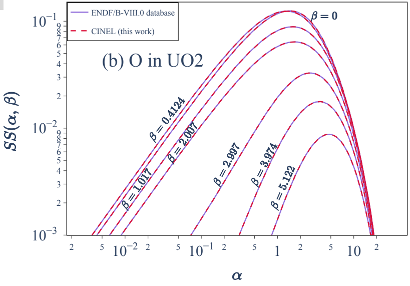

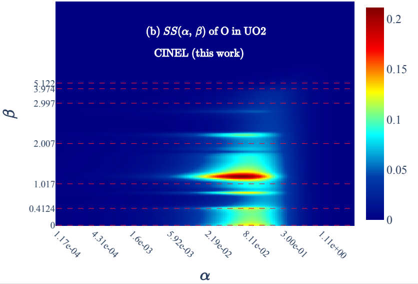

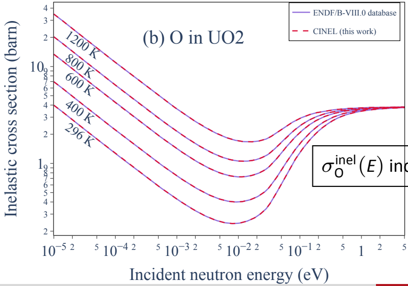

$\sigma_O^{inel}(E)$ increase with T

Numerical validations of CINEL: ^{27}Al (FCC), ^{9}Be (HCP), ^{56}Fe (BCC)

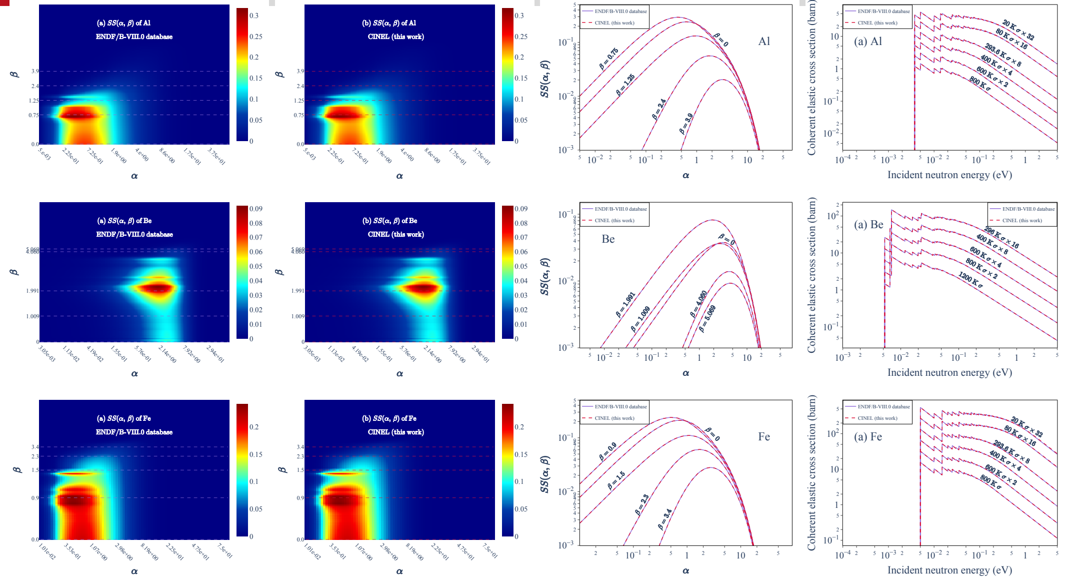

Table of Contents

D4 & D20 diffraction experiments on UO_2 performed at ILL

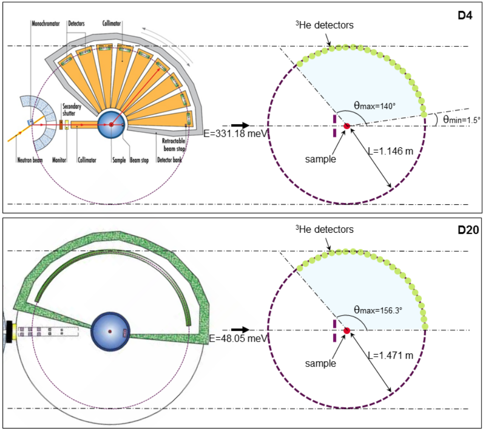

Figure: The left hand drawings represent simplified top view of the D4 and D20 diffractometers of the Institute Laue–Langevin (ILL). Those on the right hand side show the geometries introduced in the Monte-Carlo calculations.

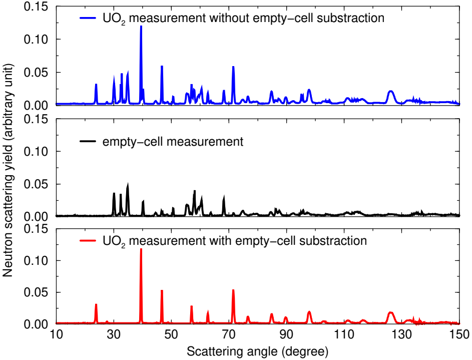

Figure: Examples of neutron diffraction patterns measured on D20 at $T = 292$ K ($E = 48.05$ meV).

Calculation scheme & PDOS measured at ILL

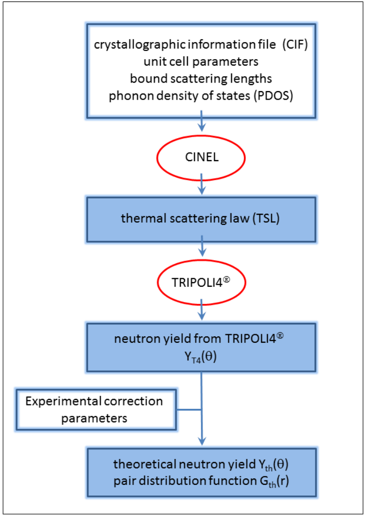

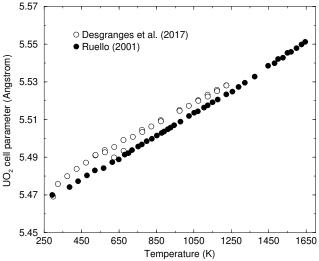

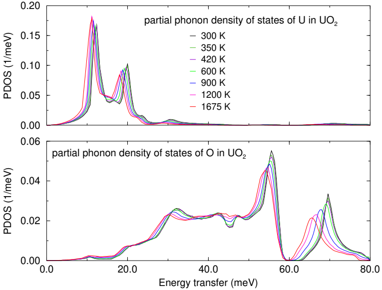

Noguere et al. (2020)

Experimental & theoretical diffraction patterns of D20

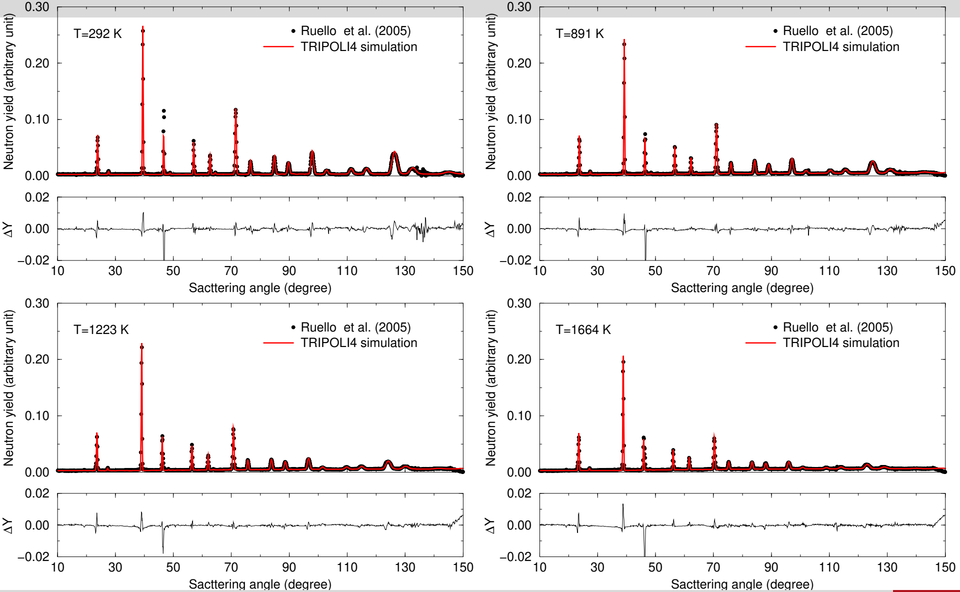

Experimental & theoretical diffraction patterns of D4

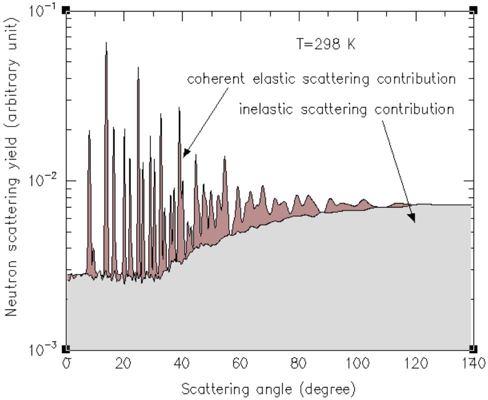

Figure: Inelastic and coherent elastic scattering contributions simulated with the TRIPOLI4® code at $T = 298$ K for D4 ($E = 331.18$ meV).

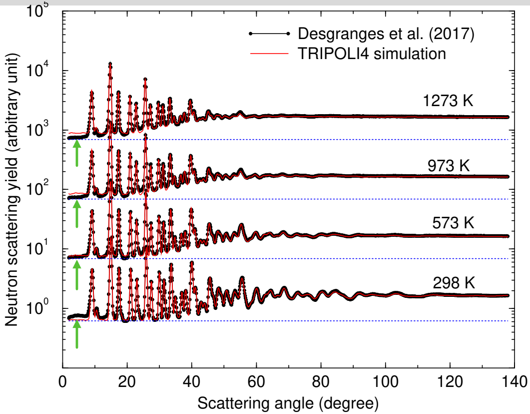

Figure: Experimental and theoretical UO2 diffraction patterns for D4 from 298 to 1273 K ($E = 331.18$ meV). The green arrows highlight the differences observed between the experiment and the theory at the forward scattering angles. The dotted blue lines show the increasing inelastic scattering contribution with the scattering angle.

Experimental & theoretical atomic pair distribution function (PDF) of D4

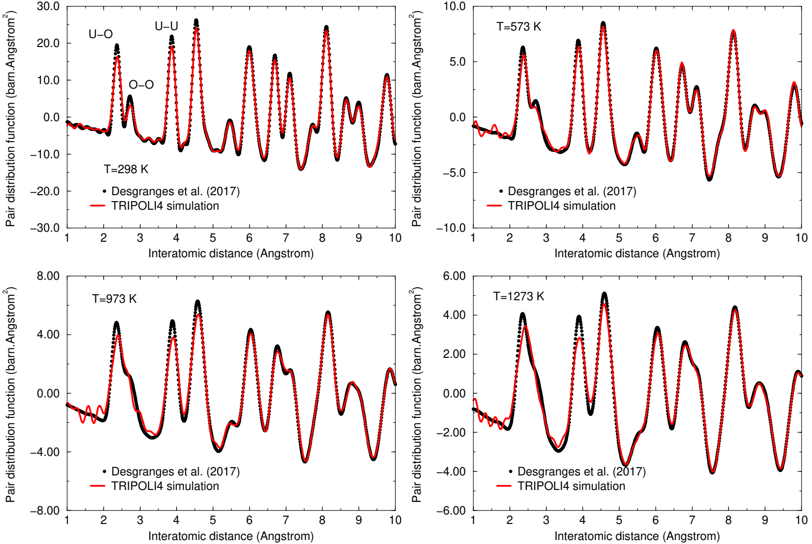

Confirmation of unexpected shortening of the U–O distance with increasing temperature reported in the literature.

Table of Contents

Conclusions

- Numerical validations of the thermal scattering law (TSL) processing code CINEL by comparing with the ENDF/B-VIII.0 database for various crystalline materials;
- Performances of the Monte-Carlo neutron transport code TRIPOLI4® with TSLs provided by CINEL, to simulate the neutron diffraction experiments on UO_2 measured at ILL up to 1664 K;
- Confirmation of the local deviation of the oxygen atoms from the average positions for UO_2 in ideal fluorite structure ($Fm\bar{3}m$ symmetry) at elevated temperatures by comparing the experimental and theoretical atomic pair distribution functions (PDF);

The neutron cross sections for UO_2, calculated with the processing code CINEL, will be delivered at the JEFF project of the OECD/NEA databank.

Perspectives

- Introduction of one-phonon correction to improve the incoherent approximation and elimination of the cubic approximation in CINEL;
- Interpretation of the background correction to be investigated.

Thank you for your attention!

References I

Cai, X.-X., & Kittelmann, T. (2020). Ncrystal: A library for thermal neutron transport. *Computer Physics Communications*, *246*, 106851. Retrieved from https://www.sciencedirect.com/science/article/pii/S0010465519302280 doi: https://doi.org/10.1016/j.cpc.2019.07.015

Cai, X.-X., Kittelmann, T., Klinkby, E., & Márquez Damián, J. (2019). Rejection-based sampling of inelastic neutron scattering. *Journal of Computational Physics*, *380*, 400-407. Retrieved from https://www.sciencedirect.com/science/article/pii/S0021999118307885 doi: https://doi.org/10.1016/j.jcp.2018.11.043

Cheng, Y. Q., Daemen, L. L., Kolesnikov, A. I., & Ramirez-Cuesta, A. J. (2019). Simulation of inelastic neutron scattering spectra using oclimax. *Journal of Chemical Theory and Computation*, *15*(3), 1974-1982. Retrieved from https://doi.org/10.1021/acs.jctc.8b01250 (PMID: 30735379) doi: 10.1021/acs.jctc.8b01250

Cheng, Y. Q., & Ramirez-Cuesta, A. J. (2020). Calculation of the thermal neutron scattering cross-section of solids using oclimax. *Journal of Chemical Theory and Computation*, *16*(8), 5212-5217. Retrieved from https://doi.org/10.1021/acs.jctc.0c00569 (PMID: 32700910) doi: 10.1021/acs.jctc.0c00569

Macfarlane, R., Muir, D. W., Boicourt, R., Kahler III, A. C., & Conlin, J. L. (2017). *The njoy nuclear data processing system, version 2016* (Tech. Rep.). Los Alamos National Lab.(LANL), Los Alamos, NM (United States).

MacFarlane, R. E. (1994, 3). New thermal neutron scattering files for endf/b-vi release 2. Retrieved from https://www.osti.gov/biblio/10192168 doi: 10.2172/10192168

Noguere, G., Scotta, J. P., Xu, S., Filhol, A., Ollivier, J., Farhi, E., … Berrod, Q. (2020, Oct). Combining density functional theory and monte carlo neutron transport calculations to study the phonon density of states of Uo_2 up to 1675 k by inelastic neutron scattering. *Phys. Rev. B*, *102*, 134312. Retrieved from https://link.aps.org/doi/10.1103/PhysRevB.102.134312 doi: 10.1103/PhysRevB.102.134312

References II

Ong, S. P., Richards, W. D., Jain, A., Hautier, G., Kocher, M., Cholia, S., … Ceder, G. (2013, February). Python Materials Genomics (pymatgen): A robust, open-source python library for materials analysis. *Computational Materials Science*, *68*, 314–319. Retrieved from http://linkinghub.elsevier.com/retrieve/pii/S0927025612006295 doi: 10.1016/j.commatsci.2012.10.028

Schober, H. (2014). An introduction to the theory of nuclear neutron scattering in condensed matter. *Journal of Neutron Research*, *17*(3-4), 109–357. Retrieved from https://content.iospress.com/download/journal-of-neutron-research/jnr016?id=journal-of-neutron-research%2Fjnr016 doi: 10.3233/JNR-140016

Sjolander, A. (1958). Multi-phonon processes in slow neutron scattering by crystals. *Arkiv Fysik*, *14*.

Squires, G. L. (2012). *Introduction to the theory of thermal neutron scattering* (3rd ed.). Cambridge University Press. doi: 10.1017/CBO9781139107808

Trkov, A., & Brown, D. A. (2018). *Endf-6 formats manual: Data formats and procedures for the evaluated nuclear data files* (Tech. Rep.). Brookhaven National Lab.(BNL), Upton, NY (United States).

Wormald, J. L., Fleming, N. C., Hawari, A. I., & Zerkle, M. L. (2021). Generation of the thermal scattering law of uranium dioxide with ab initio lattice dynamics to capture crystal binding effects on neutron interactions. *Nuclear Science and Engineering*, *195*(3), 227-238. Retrieved from https://doi.org/10.1080/00295639.2020.1820826 doi: 10.1080/00295639.2020.1820826

Zhu, Y., & Hawari, A. I. (2018). Full law analysis scattering system hub (flassh). In *Proc. physor* (pp. 22–26).